IEEE Photonics Journal
An IEEE Photonics Society Publication

Open Access

Vertical Second Harmonic Generation in Asymmetric Dielectric Nanoantennas

Volume 12, Number 3, June 2020

Davide Rocco
Carlo Gigli
Luca Carletti
Giuseppe Marino
Maria Antonietta Vincenti
Giuseppe Leo
Costantino
De Angelis

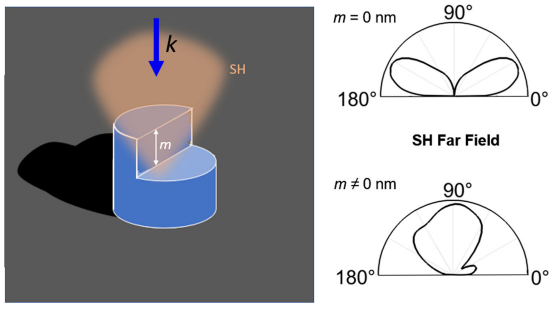

DOI: 10.1109/JPHOT.2020.2988502

Vertical Second Harmonic Generation in Asymmetric Dielectric Nanoantennas

Davide Rocco,[1,2] Carlo Gigli,[3] Luca Carletti,[4] Giuseppe Marino,[3] Maria Antonietta Vincenti,[1] Giuseppe Leo,[3] and Costantino De Angelis[1,2]

[1]Department of Information Engineering, University of Brescia, via Branze 38, Brescia 25123, Italy
[2]National Institute of Optics, CNR-INO, via Branze 45, Brescia 25123, Italy
[3]Matériaux et Phénomènes Quantiques, Université de Paris, 10 Rue Alice Domon et Léonie Duquet 75013, Paris, France
[4]Department of Information Engineering, University of Padova, via Gradenigo 6, Padova 35131, Italy

DOI:10.1109/JPHOT.2020.2988502

Manuscript received March 13, 2020; revised April 10, 2020; accepted April 14, 2020. Date of publication April 20, 2020; date of current version May 15, 2020. This work was supported in part by MIUR Ministero dell'Istruzione, dell'Università e della Ricerca (2017MP7F8F) and in part by CNR Consiglio Nazionale delle Ricerche (Joint Lab Project). Corresponding author: Davide Rocco (e-mail: d.rocco003@unibs.it).

Abstract: High-permittivity III–V semiconductor nanocavities have shown huge potential for enhanced nonlinear light–matter interactions at the nanoscale. In particular, Second Harmonic (SH) generation in AlGaAs nanoantennas can be extremely efficient; however, vertical emission is difficult to achieve, due to the zincblende $\chi^{(2)}$ tensor and epitaxially growth on (100) substrates. Here, we demonstrate that we can shape the second harmonic radiation pattern from a single AlGaAs nanostructure by exploiting a geometrical symmetry breaking optimization approach. The optimized design allows to redirect the SH signal toward the normal direction and to increase the SH power collection efficiency by 2 orders of magnitude in a small numerical aperture of 0.1 with respect to the symmetrical counterpart structure.

Index Terms: Nonlinear optics devices, optical harmonic generation, optical resonator.

1. Introduction

Optical antennas have recently attracted a lot of attention due to their potential application in different research areas [1]–[3]. Significantly, their capability to strongly confine light at the sub-wavelength scale makes optical antennas particularly desirable for various applications [4]–[8]. All-dielectric optical resonators present two fundamental properties that are absent in plasmonics: extremely low losses in the infra-red spectral region, which results in high radiation efficiency, and multipolar nature of both electric and magnetic internal resonant fields [9]–[11]. Furthermore, optically induced Mie-like resonances sustained by dielectric nanostructures, show near-field distributions with relatively high enhancement inside the nanoantennas due to multipolar interference effects [12,13]. These kinds of structures have thus emerged as a promising building block to improve the nonlinear conversion processes such as Second or Third Harmonic generation (SHG/THG) at the nanoscale [14]–[21]. Among the class of III–V semiconductors, AlGaAs is of mentionable interest as it exhibits high permittivity and large second-order nonlinear susceptibility

[14]. Recently, SHG efficiency of the order of 10^{-5} was demonstrated in AlGaAs on AlOx platform [15] and then different studies were proposed to maximize the total SH signal [22]–[24]. Despite the high conversion efficiencies, what all these structures have in common is their SH radiation pattern, which presents a null in the forward and backward directions when the pump is impinging at normal-incidence [25, 26]. This peculiarity is related to the symmetry of the AlGaAs second-order nonlinear susceptibility. As a matter of fact, engineering the SH radiation pattern is strongly necessary in a lot of low-power and low-cost applications such as biological or chemical sensing [27]–[30]. It is known that the symmetry of the system needs to be weakened to shape the SH radiation into more suitable patterns with high emission in the normal direction and following this concept different studies have been already carried out [31, 32]. Different approaches have been recently proposed to reshape the SH generation pattern. One possibility is to reduce the system symmetry by tilting the pump beam with respect to the main crystal axis [33]. An alternative approach consists of creating a surrounding grating structure that enables the redirection of the coherent SH radiation emitted at grazing angles from the optical antenna toward its normal [25]. Finally, the fabrication of AlGaAs nanodisks with crystalline axis rotated with respect to the global coordinate system has been proposed by addressing epitaxial growth on either (111) or (110) substrates [34], [35]. However, the former is not easy to obtain because it necessitates elevate growth temperature with a narrow growth window, thus achieving an irregular morphology, while both (111) and (110) substrates are not standard in diode laser technology and reduce the overall compatibility of the related metastructures with a full optoelectronic integration. Here, we suggest an alternative approach to reshape the SH radiation pattern with a pump at normal incidence and the common (100) crystalline axis orientation of the dielectric structure. Thus, our design can be realized with minimal complexity in the nanoantenna fabrication and experimental implementation. We propose a geometrical symmetry broken structure that guarantees an enhancement of more than two orders of magnitude in a small numerical aperture (NA $= 0.1$) around the normal direction with respect to its symmetrical counterpart structure.

2. Results and Discussion

The basic idea implemented in this work is strictly related to the filtering mechanism used in dielectric asymmetric grating. Indeed, it is possible to fabricate a long-wavelength infrared narrowband transmission filter using an asymmetric subwavelength dielectric grating. The two-step grating geometry guarantees a normal-incidence response, overcoming the limitations of rectangular gratings [36]. Following the same approach, we rescale the aforementioned concept to dielectric nanoantennas. Let us consider as a reference structure a nanodisk made of AlGaAs with a radius $r = 205$ nm and a total height $h = 400$ nm. For these dimensions the dielectric nanocylinder exhibits a magnetic dipolar resonance around 1550 nm, as already reported in [15]. We now cut the cylinder in two regions with a plane parallel to its axis [see Fig. 1(a)], and call m the height difference between the two resonator regions [see Fig. 1(b)]. The proposed structure can be fabricated starting from an epitaxial growth of AlGaAs on GaAs substrate with an analogue approach as reported in [15]. Thus, at the end of the fabrication procedure, the nanodisk is placed over an AlOx substrate. To emulate the linear and nonlinear behaviour of the antenna under test we perform Finite Element Method simulations in COMSOL Multiphysics. The AlGaAs permittivity is supposed to be the same as in [37], whereas for the AlOx layer we consider a wavelength independent refractive index equal to 1.6 [15]. The excitation beam is assumed to be a linearly polarized plane wave, at a wavelength of 1550 nm, with a pump intensity equal to 1.6 GW/cm^2.

The analysis of the SHG mechanism is implemented by using the nonlinear polarization induced by the nonlinear susceptibility of the second order, $\chi^{(2)}$. The latter is supposed to have a value of 200 pm/V [15]. Moreover, due to the AlGaAs zinc-blende crystalline structure, the only non-zero elements of the nonlinear susceptibility tensor $\chi_{ijk}^{(2)}$ are obtained for $i \neq j \neq k$ [14]. For simplicity, let us start by analyzing just two different cases. In the first one, the AlGaAs crystalline axes are oriented along the reference system of the laboratory [i.e., $\theta = 0$, see Fig. 1(c)] while the second one displays $\pi/4$ rotation between the AlGaAs axis and the laboratory reference, i.e., $\theta = \pi/4$.

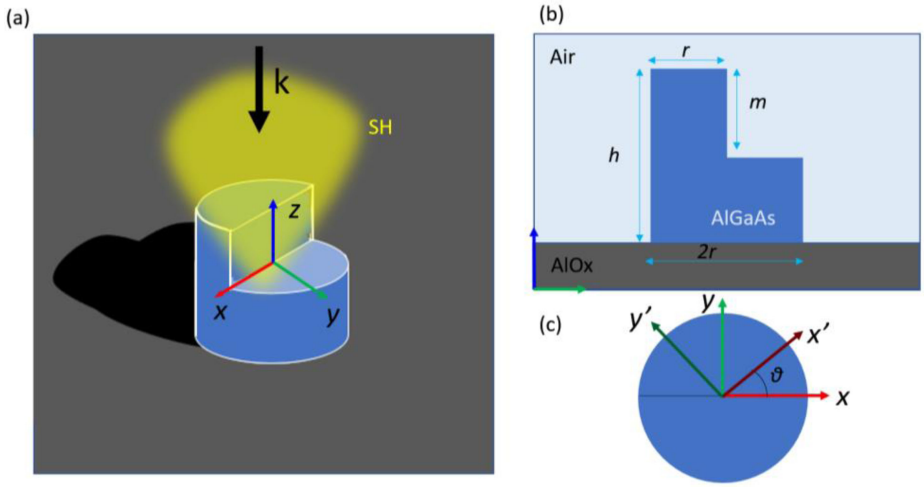

Fig. 1. (a) Sketch of the proposed structure and (b) relative dimensions. (c) The considered orientation of the AlGaAs crystalline axis.

These two crystalline axis configurations thus differ only by an in-plane rotation in the *xy* plane. We thus performed a study of the SHG when *m* is varying between 0 nm (unperturbed pillar) and 400 nm. Moreover, since the structure is symmetry-broken when $m \neq 0$, we expect to redirect some SH signal towards the normal direction. Thus, we define the SHG gain (ρ_{SHG}) as the SH collected power in a small NA (i.e., equal to 0.1) when $m \neq 0$ with respect to the SH collected power in the same NA for the full isolated pillar ($m = 0$). It is known that when $m = 0$ (i.e., full isolated pillar) the SH signal is emitted solely at large angles [see inset of Fig. 2(a)], while no signal is radiated along the normal direction despite of the polarization. This property has been noticed in previous investigations carried out on analogous devices and is connected to the symmetry of the nonlinear $\chi^{(2)}$ tensor and the excitation light beam. By increasing *m,* the symmetry of the structure is broken and the modification in SH radiation pattern is thus possible. Please also notice that in the case of $m \neq 0$ the structure is no more symmetric in the *xy* plane, thus different behavior is expected for different incident polarization of the pump. Still, for sake of simplicity, we limit ourselves to study the nonlinear performances when the incident plane wave is polarized along *x* or *y*. Figs. 2(a) and (b) show the obtained results for the two considered input polarizations by varying *m*. Firstly, we consider the case of $\theta = 0$ rad, where θ is the angle between the E-field vector and the *x*-axis. In the case of *x* polarized light the maximum reshaping along the normal direction is obtained for $m = 200$ nm, see red curve of Fig. 2(a). The associated SH mode pattern is reported in Fig. 2(c). In this configuration, an increase of two orders of magnitude in the SH generation measured in a small NA is obtained, more precisely ρ_{SHG} reaches the maximum value of 195. Instead, for *y* polarized light the maximum ρ_{SHG} (equal to 53) is obtained for $m = 150$, see Figs. 2(b) and (d). Although at the two optimal *m* values (200 nm and 150 nm) the SH shows a similar radiation pattern, as illustrated by the insets of Fig. 2, it should be noted that the nonlinear generation signal is about 4 times more efficient for incident light polarized along the height discrepancy direction due to smaller electric field perturbation at the fundamental wavelength. This is corroborated by the SHG efficiency that results 1.6×10^{-5} for $m = 200$ nm and *x* polarized excitation whereas the nonlinear efficiency is 4×10^{-6} when $m = 150$ nm for the other input polarization. Secondly, we analyze the case when $\theta = \pi/4$ rad. The gain in the SH, ρ_{SHG}, is always less than 30 for the *x* polarized plane wave and less than 6 for the *y* polarized excitation, as illustrated by the blue curve of Figure 2. Thus, in the following we report the results of the most promising case of $\theta = 0$ rad.

The trend observed in Fig. 2 can be easily appreciated in the far-field images that we calculate for the incident light polarized along *x* (Fig. 2(a)) or *y* (Fig. 2(b)) for $m = 200$ nm and $m = 150$ nm respectively, as depicted in Fig. 3. We observe for both incident polarization a noticeable angular

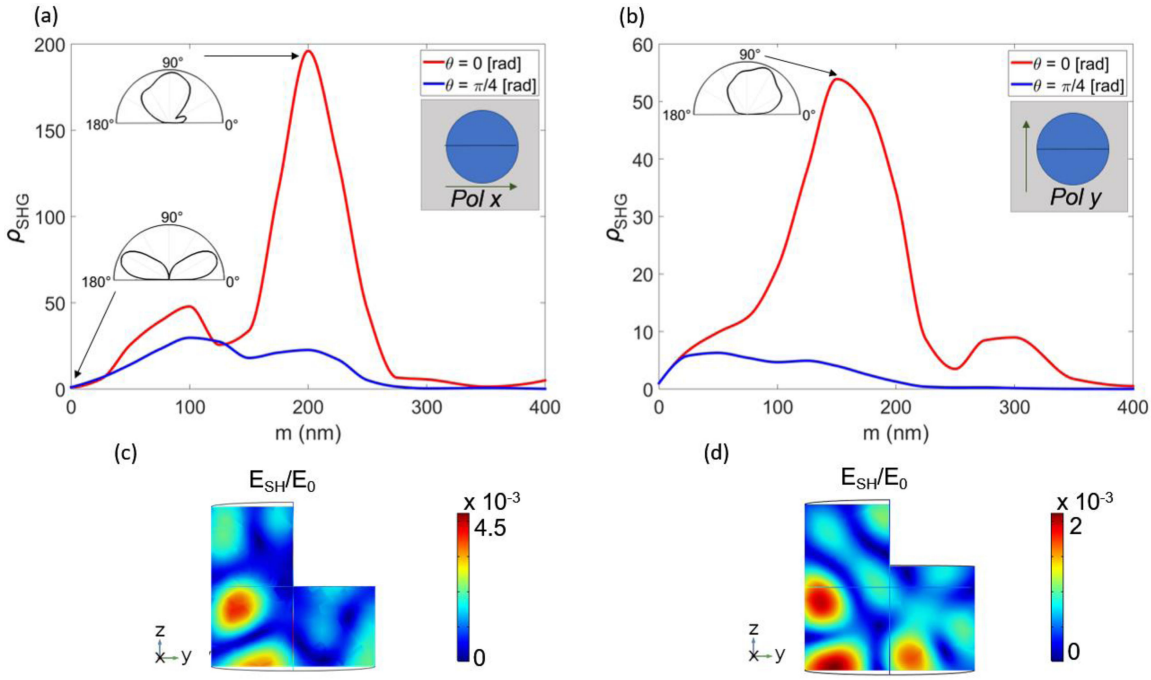

Fig. 2. The SH gain, ρ_{SHG}, for (a) *x* or (b) *y* polarized incident light as a function of the height difference *m*. The red curves refer to the case of AlGaAs crystalline axis oriented as the laboratory reference ($\theta = 0$) instead the blue lines represent the case of $\pi/4$ rotation of the crystalline axis in the *xy* plane. The insets on the left represent the SH radiation diagram in the air region in the *zx* plane at different *m* values. The normalized nonlinear mode pattern (c) for *m* equal to 200 nm with *x*-polarized incident light ($\theta = 0$ rad) and (d) for $m = 150$ nm with *y*-polarized plane wave excitation ($\theta = 0$ rad).

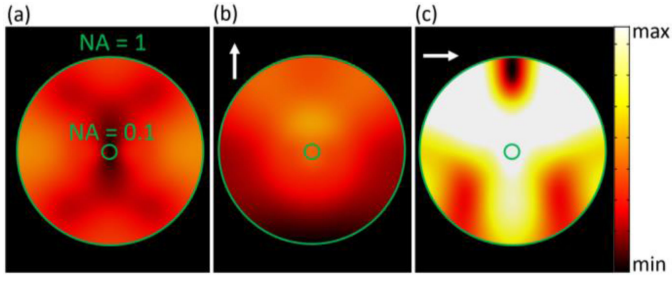

Fig. 3. Far-field images (*xy* plane) of the SH radiation emitted in the backward direction for (a) the isolated full pillar ($m = 0$ nm), asymmetric structure with (b) $m = 150$ nm and (c) $m = 200$ nm. The white arrows indicate the polarization of the incident light at the fundamental wavelength. The green circles represent the NA. The plots are reported using the same scalebar.

redistribution of the SH pattern from two lateral lobes of the full pillar (Fig. 3(a)) into a central lobe (Figs. 3(b) and (c)) of the optimized asymmetric structures. We recall that, for the full isolate pillar, the nonlinear currents in the opposite halves of the resonator present a phase shift that is translated into a destructive interference in the far-field resulting in the so called “doughnut-shaped” radiation pattern. Thus, the isolated AlGaAs nanodisk generates a SH signal that mostly radiates the power to the sides and with low directivity, therefore complicating the collection of the SHG light using finite numerical aperture objectives [25, 26, 34].

To understand the observed behavior in the asymmetric structure, we analyze the nonlinear currents generated inside the crystal. We recall that the *i*-th component of the nonlinear current

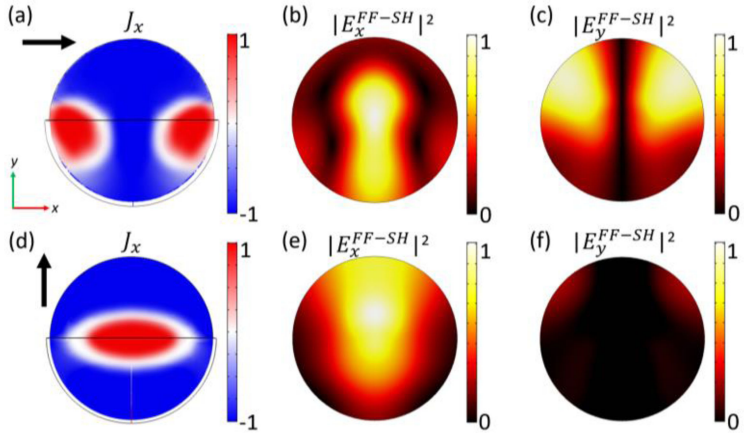

Fig. 4. Normalized *x*-component (real part) of the nonlinear currents induced in the structure (a) for a *x* polarized light and $m = 200$ nm and (d) for *y* incident polarized field and $m = 150$ nm. The *x* [(b), (e)] and *y* [(c), (f)] component of the SH Far Field signal in a NA $= 1$ for the two optimal cases of $m = 200$ nm and $m = 150$ nm respectively. The black arrows indicate the incident light polarization.

density is determined as $J_i = j\omega_{SH}\varepsilon_0\ \chi^{(2)}\ E_{FW,j}\ E_{FW,k}$ with $i \neq j \neq k$ where ε_0 is the vacuum permittivity, ω_{SH} the angular frequency of the SH and $E_{FW,j}$ is the *j*-th component of the electric field at the fundamental wavelength [14]. For the two optimized cases analyzed in Figs. 2(b) and (c), the J_x, J_y and J_z have similar absolute values. Since the SH field emitted in the NA $= 0.1$ is polarized along the *x*-axis direction, we analyze the nonlinear current with the same orientation, as shown in Fig. 4. The *x*-component of the nonlinear currents presents an even-symmetry distribution that is consistent with a SH mode having a central lobe emission [33]. Thus, the proposed optimized asymmetric structure successfully breaks the field symmetry inside the dielectric structure and produces SH nonlinear currents which manifest a symmetry that is consistent with modes emitting in the vertical direction.

To gain a deeper understanding of the nonlinear behavior of the above structure, let us also resort to the Quasi Normal-Modes (QNMs) formalism. One of its key outcomes is the possibility to reconstruct the SH field with a closed-form expression involving only few dominant resonances [38], [39]. A set of QNMs around fundamental ($\lambda_{FF} = 1550$ nm) and second harmonic wavelengths ($\lambda_{SH} = 775$ nm) is computed with freeware toolbox QNMEig [40]. A single-pole Lorentzian is used to fit the empiric model for AlGaAs refractive index in [37]. Using the formalism presented in [38,40], the excitation coefficients of the computed eigenmodes for the optimized structure ($m = 200$ nm, *x* polarized light) are retrieved and the extinction cross section at SH is reconstructed. The result is truncated to the four most excited QNMs. A systematic analysis of the convergence performance of QNM expansions can be found in [40]. The obtained nonlinear extinction spectrum is depicted in Fig. 5 together with all the four most excited QNMs contributions (called SH1-SH4).

As can be seen in Figure 5, there is a dominant SHG peak. The powerful nonlinear QNM expansion allow us to directly assess the contribution of every individual QNM to the SH extinction, thereby revealing that the dominant mode is only SH1 (light blue dotted line in Fig. 5(a)). The linear electric field map around the frequencies of SH peak and the corresponding fundamental frequency are reported in Fig. 5(b), instead the near field maps associated with SH1 are reported in Fig. 5(c). It is evident that the latter QNM almost perfectly matches with the exact near field distribution obtained with fully vectorial simulation, see Fig. 5(d). Also, the far-field images of the SH1 mode (computed applying the near to far-field transformation described in [41]) has a high similarity with the corresponding images coming from a full wave numerical result (see Figs. 5(e) and (f) for comparison]). In other words, the symmetry breaking of the structure is optimized to well excite a mode at the SH with a non-zero SH component in the normal direction and thus to boost the collected SH power in a small NA.

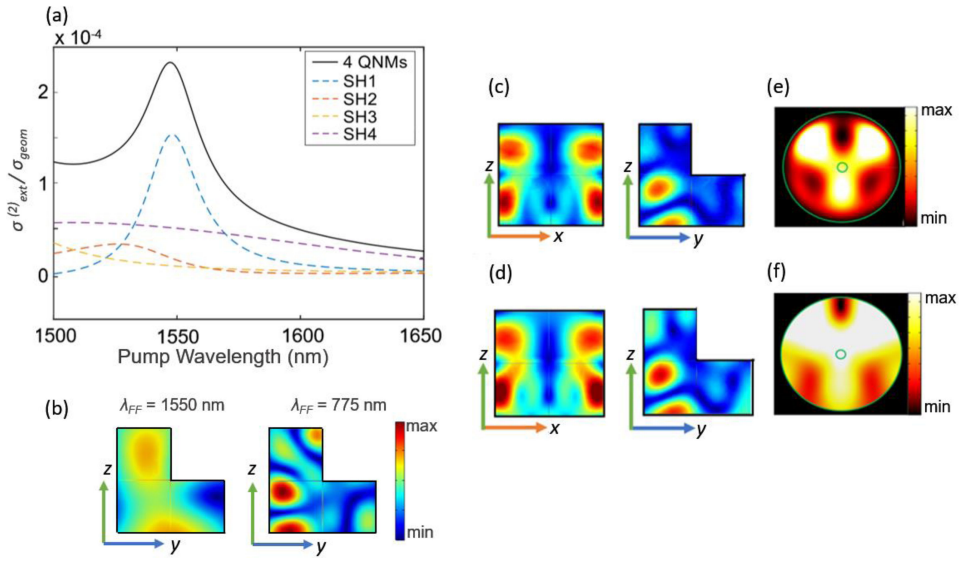

Fig. 5. (a) SHG extinction efficiencies for the optimized structure with $m = 200$ nm, $r = 205$ nm, and $h = 400$ nm. The approximate cross section (black solid line) is reconstructed with four dominant QNMs (SH1-SH4). (b) The linear electric field distribution inside the nanoantennas for incident pump wavelength equal to 1550 nm and 775 nm respectively. (c) The near field distribution of SH1 and (d) the near field map of the exact numerical results. (e) The far-field image (*xy* plane) of the SH1 mode and (f) the back focal as obtained in Comsol. The inner green circles represent a NA equal to 0.1 instead the external one a NA equal to 1.

3. Conclusions

In this work, we have developed a simple approach, based on symmetry breaking in the geometrical parameters of (100) AlGaAs cylindrical nanoantenna, to achieve SHG in the normal direction. In particular, we have shown that letting the heights of the two semi-cylinders vary, enables to effectively engineer the radiation pattern of the nonlinear SH signal. For the optimized structure, we demonstrate that the collected power in a small numerical aperture (NA = 0.1) in the backward direction increases by more than two orders of magnitude with respect to the case of the unperturbed nanocylinder. Among the different options for obtaining such second harmonic normal generation, including the fabrication of (111) or (110) AlGaAs nanoantennas, our strategy optimally combines record directionality and full compatibility with (100) AlGaAs optoelectronic integration.

Acknowledgment

The authors wish to thank the anonymous reviewers for their valuable suggestions.

References

[1] A. E. Krasnok *et al.*, "All-dielectric optical nanoantennas," *Opt. Express*, vol. 20, no. 18, pp. 20599–20604, Aug. 2012.
[2] A. E. Krasnok, I. S. Maksymov, A. I. Denisyuk, P. A. Belov, A. E. Miroshnichenko, C. R. Simovski, and Y. S. Kivshar, "Optical nanoantennas," *Phys-Usp*, vol. 56, no. 6, pp. 539–564, Nov. 2013.
[3] M. L. Brongersma, "Plasmonics: Engineering optical nanoantennas," *Nat. Photo.*, vol. 2, no. 5, pp. 270–272, May 2008.
[4] A. Sundaramurthy, P. J. Schuck, N. R. Conley, D. P. Fromm, G. S. Kino, and W. E. Moerner, "Toward nanometer-scale optical photolithography: Utilizing the near-field of bowtie optical nanoantennas," *Nano Lett.*, vol. 6, no. 3, pp. 355–360, Feb. 2006.
[5] C. D'Andrea *et al.*, "Optical nanoantennas for multibrand surface-enhanced infrared and Raman spectroscopy," *ACS Nano*, vol. 7, no. 4, pp. 3522–3531, Mar. 2013.
[6] A. Tittl, C. Kremers, J. Dorfmüller, D. N. Chigrin, and H. Giessen, "Spectral shifts in optical nanoantenna-enhanced hydrogen sensors," *Opt. Mat. Express*, vol. 2, no. 2, pp. 111–118, Jan. 2012.
[7] T. Grosjean, M. Mivelle, F. I. Baida, G. W. Burr, and U. C. Fischer, "Diabolo nanoantenna for enhancing and confining the magnetic optical field," *Nano Lett.*, vol. 11, no. 3, pp. 1109–1013 Feb. 2011.

[8] M. Caldarola *et al.*, "Non-plasmonic nanoantennas for surface enhanced spectroscopies with ultra-low heat conversion," *Nat. Commun.*, vol. 6, no. 1, pp. 1–8, Aug. 2015.
[9] N. de Sousa, L. S. Froufe-Pérez, J. J. Sáenz, and A. García-Martín, "Magneto-optical activity in high index dielectric nanoantennas," *Sci. Rep.*, vol. 6, p. 30803, Aug. 2016.
[10] A. I. Kuznetsov, A. E. Miroshnichenko, M. L. Brongersma, Y. S. Kivshar, and B. Luk'yanchuk, "Optically resonant dielectric nanostructures," *Science*, vol. 354, no. 6314, pp. aag2472-1–aag2472-8, Nov. 2016.
[11] D. Rocco, L. Carletti, A. Locatelli, and C. De Angelis, "Controlling the directivity of all-dielectric nanoantennas excited by integrated quantum emitters," *JOSA B*, vol.34, no. 9, pp. 1918–1922, Sep. 2017.
[12] Y. Yang, V. A. Zenin, and S. I. Bozhevolnyi, "Anapole-assisted strong field enhancement in individual all-dielectric nanostructures," *ACS Photonics*, vol. 5, no. 5, pp. 1960–1966, Mar. 2018.
[13] A. E. Miroshnichenko *et al.*, "Nonradiating anapole modes in dielectric nanoparticles," *Nat. Comm.*, vol. 6, no. 1, pp. 1–8, Aug. 2015.
[14] L. Carletti, A. Locatelli, O. Stepanenko, G. Leo, and C. De Angelis, "Enhanced second-harmonic generation from magnetic resonance in AlGaAs nanoantennas," *Opt. Express*, vol. 23, no. 20, pp. 26544–26550, Oct. 2015.
[15] V. F. Gili *et al.*, "Monolithic AlGaAs second-harmonic nanoantennas," *Opt. Express*, vol. 24, no. 14, pp. 15965–15971, Jul. 2016.
[16] S. S. Kruk *et al.*, *Nano Lett.*, vol. 17, no. 6, pp. 3914–3918, May 2017.
[17] L. Xu *et al.*, "Boosting third-harmonic generation by a mirror-enhanced anapole resonator," *Light Sci. Appl.*, vol. 7, no. 1, pp. 1–8, Jul. 2018.
[18] T. Shibanuma, G. Grinblat, P. Albella, and S. A. Maier, "Efficient third harmonic generation from metal–dielectric hybrid nanoantennas," *Nano Lett.*, vol. 17, no. 4, pp. 2647–2651, Mar. 2017.
[19] M. Timofeeva *et al.*, "Anapoles in free-standing III–V nanodisks enhancing second-harmonic generation," *Nano Lett.*, vol.18, no. 6, pp. 3695–3702, May 2018.
[20] L. Wang *et al.*, "Shaping the third-harmonic radiation from silicon nanodimers," *Nanoscale*, vol. 9, no. 6, pp. 2201–2206, Jan. 2017.
[21] M. R. Shcherbakov *et al.*, "Enhanced third-harmonic generation in silicon nanoparticles driven by magnetic response," *Nano Lett.*, vol. 14, no. 11, pp. 6488–6492, Oct. 2014.
[22] V. F. Gili *et al.*, "Metal–dielectric hybrid nanoantennas for efficient frequency conversion at the anapole mode," *Beilstein. J. Nanotechnol.*, vol. 9, no. 1, pp. 2306–2314, Aug. 2018.
[23] D. Rocco, M. A. Vincenti, and C. De Angelis, "Boosting Second Harmonic Radiation from AlGaAs Nanoantennas with Epsilon-Near-Zero Materials," *Appl. Sci.*, vol. 8, no. 11, p. 2212, Nov. 2018.
[24] K. Koshelev *et al.*, "Subwavelength dielectric resonators for nonlinear nanophotonics," *Science*, vol. 367, no. 6475, pp. 288–292, Jan. 2020.
[25] L. Ghirardini *et al.*, "Shaping the nonlinear emission pattern of a dielectric nanoantenna by integrated holographic gratings," *Nano Lett.*, vol. 18, no. 11, pp. 6750–6755, Oct. 2018.
[26] R. Camacho-Morales *et al.*, "Nonlinear generation of vector beams from AlGaAs nanoantennas," *Nano Lett.*, vol. 16, no. 11, pp. 7191–7197, Oct. 2016.
[27] D. Rocco, L. Di Donato, G. Sorbello, and C. De Angelis, "Second harmonic beam shaping and sensing in dielectric bow-tie antenna via convex Optimization array synthesis approach," *Electronics*, vol. 8, no. 8, p. 901, Aug. 2019.
[28] J. Butet, I. Russier-Antoine, C. Jonin, N. Lascoux, E. Benichou, and P. F. Brever, "Sensing with multipolar second harmonic generation from spherical metallic nanoparticles," *Nano Lett.*, vol.12, no. 3, pp. 1697–1701, Feb. 2012.
[29] T. Pons, L. Moreaux, O. Mongin, M. H. Blanchard-Desce, and J. Mertz, "Mechanisms of membrane potential sensing with second-harmonic generation microscopy," *J. Biomed. Opt.*, vol. 8, no. 3, pp. 428–432, Jul. 2003.
[30] S. N. Son, J. J. Song, J. U. Krang, and C. S. Kim, "Simultaneous second harmonic generation of multiple wavelength laser outputs for medical sensing," *Sensors*, vol. 11, no. 6, pp. 6125–6130, Jun. 2011.
[31] L. Carletti *et al.*, "Controlling second-harmonic generation at the nanoscale with monolithic AlGaAs-on-AlOx antennas," *Nanotechnology*, vol. 28, no. 11, p. 114005, Feb. 2017.
[32] G. Marino, C. Gigli, D. Rocco, A. Lemaître, C. De Angelis, and G. Leo, "Zero-order second harmonic generation from AlGaAs-on-insulator metasurfaces," *ACS Photonics*, vol. 6, no. 5, pp. 1226–1231, Apr. 2019.
[33] L. Carletti *et al.*, "Nonlinear goniometry by second-harmonic generation in algaas nanoantennas," *ACS Photonics*, vol. 5, no. 11, pp. 4386–4392, Nov. 2018.
[34] J. D. Sautter *et al.*, "Tailoring Second-Harmonic Emission from (111)-GaAs Nanoantennas," *Nano Lett.*, vol. 19, no. 6, pp. 3905–3911 May 2019.
[35] L. Xu *et al.*, "Forward and backward switching of nonlinear unidirectional emission from gaas nanoantennas," *ACS Nano*, Dec. 2019.
[36] M. Scherr, M. Barrow, and J. Phillips, "Long-wavelength infrared transmission filters via two-step subwavelength dielectric gratings," *Opt. Letters*, vol. 42, no. 3, pp. 518–521 Feb. 2017.
[37] S. Gehrsitz, F. K. Reinhart, C. Gourgon, N. Herres, A. Vonlanthen, and H. Sigg, "The refractive index of AlxGa1−xAs below the band gap: Accurate determination and empirical modeling," *J. Appl. Phys.*, vol. 87, no. 11, pp. 7825–7837, May 2000.
[38] C. Gigli, T. Wu, G. Marino, A. Borne, G. Leo, and P. Lalanne, "Quasinormal-mode modeling and design in nonlinear nano-optics," *arXiv:1911.06373*, Nov. 2019.
[39] P. Lalanne, W. Yan, K. Vynck, C. Sauvan, and J. P. Hugonin, "Light interaction with photonic and plasmonic resonances," *Laser Photonics Rev.*, vol. 12, no. 5, p. 1700113, Apr. 2018.
[40] W. Yan, R. Faggiani, and P. Lalanne, "Rigorous modal analysis of plasmonic nanoresonators," *Phys. Rev. B*, vol. 97, no. 20, p. 205422, May 2018.
[41] J. Yang, J. P. Hugonin, and P. Lalanne, "Near-to-far field transformations for radiative and guided waves," *ACS Photonics*, vol. 3, no. 3, pp. 395–402, Feb. 2016.